SEMARAK ILMU PUBLISHING

Semarak International Journal of Fundamental and Applied Mathematics

Journal homepage:
https://semarakilmu.my/index.php/sijfam
ISSN: 3030-5527

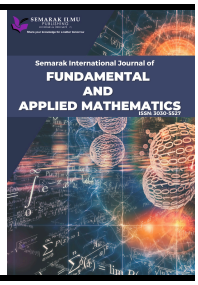

Effects of Uniform and Non-Uniform Magnetic Fields on Magnetised Fluid Flow over an Inclined Extending Plate

Nur Ilyana Kamis[1], Noraihan Afiqah Rawi[1,*], Lim Yeou Jiann[1], Sharidan Shafie[1]

[1] Department of Mathematical Sciences, Faculty of Science, Universiti Teknologi Malaysia, 81310 Skudai, Johor, Malaysia

ARTICLE INFO

Article history:
Received 15 December 2025
Received in revised form 29 January 2026
Accepted 30 January 2026
Available online 1 February 2026

Keywords:
MHD effect; FHD effect; dual ferrofluid, inclined, bvp4c

ABSTRACT

Nanoparticle-based fluids exhibit significant potential for enhancing the efficiency of solar thermal systems. Ferrofluids, characterised by high thermal conductivity and strong magnetic responsiveness, can substantially improve heat absorption and the overall performance of solar collector plates. This study investigates the influence of magnetic fields on the flow behaviour and heat transfer characteristics of a ferrofluid containing ferrite and cobalt ferrite nanoparticles, dispersed in an equal mixture of ethylene glycol and water, over an inclined stretching plate. Uniform magnetic fields are employed to examine magnetohydrodynamic (MHD) effects, while non-uniform magnetic fields are considered to capture ferrohydrodynamic (FHD) behaviour. The governing partial differential equations are transformed into a system of ordinary differential equations using similarity transformations and are subsequently solved numerically using the bvp4c function in MATLAB. The results indicate that uniform magnetic fields significantly decelerate the fluid motion, as compared to non-uniform magnetic fields. The temperature profile increases more markedly under MHD effects compared to FHD effects. In contrast, stronger magnetic fields increase shear stress while suppressing heat transfer. These findings provide valuable insights for the design and optimization of solar collector plates, enabling improved thermal efficiency and stable system operation.

1. Introduction

Solar collector plates, as shown in Figure 1 are the core components of solar thermal systems, serving as the primary surfaces for absorbing incident solar radiation and converting it into usable thermal energy [1]. The efficiency of these plates depends not only on the material and geometry of the plate but also on the effectiveness of heat transfer to the working fluid. Suman *et al.,* [2] highlighted three common strategies to enhance collector performance. The initial strategy focuses on improving heat transfer between the collector plate and the working fluid through surface modification. The second involves applying coatings to the absorber to maximise solar radiation absorption. The third strategy is to increase the thermal conductivity of the working fluid by

* *Corresponding author.*
E-mail address: noraihanafiqah@utm.my

introducing nanoparticles, thereby employing nanofluids as the heat transfer medium [2]. The limited thermal conductivity of conventional fluids restricts convective heat transfer from the plate to the fluid, presenting a critical obstacle to achieving high overall system efficiency.

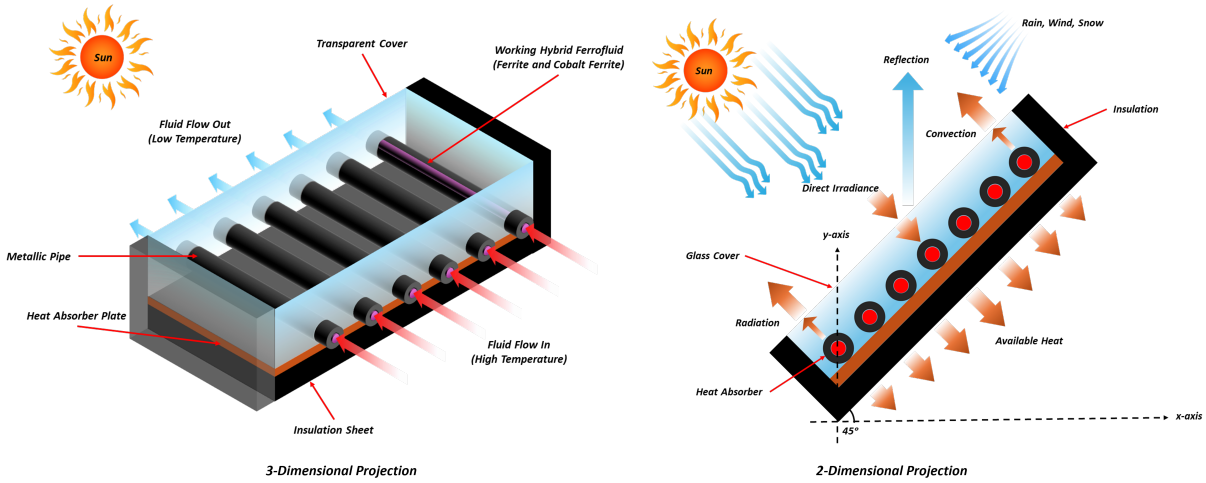

Fig. 1. Solar collector plate geometry with heat transfer processes [3,4]

To address these limitations, a dual ferrofluid can be employed as the working fluid. This fluid comprises a mixture of various magnetic nanoparticles uniformly dispersed in a base fluid [5]. The combination of the thermal and magnetic characteristics of these nanoparticles results in higher thermal conductivity, stronger magnetisation, and improved stability compared to conventional nanofluids [6]. As a result, the use of such a magnetised fluid in solar collectors enhances heat transfer, thereby increasing thermal efficiency and solar energy absorption [7]. When exposed to a magnetic field, the dual ferrofluid experiences temperature-dependent forces that generate additional fluid motion, a phenomenon known as thermomagnetic convection [8]. The type of magnetic field governs the characteristics of the fluid. The uniform magnetic fields primarily induce the magnetohydrodynamic (MHD) effect. In contrast, non-uniform magnetic fields such as those generated by magnetic dipoles create spatial gradients that lead to the ferrohydrodynamic (FHD) effect. These effects influence the magnetised fluid motion through its magnetisation [9]. A comparison of these two effects is presented in Table 1 [10,11]. The synergistic effects further strengthen convective heat transfer from the solar collector plate, providing an efficient approach to enhancing the thermal efficiency of the system.

Table 1
Comparison between MHD and FHD effects

Features	**MHD Effect**	**FHD Effect**
Definition	The influence of externally applied uniform magnetic fields from external devices like coils or current-carrying wires on electrically conducting fluids (plasma and water), inducing an electric current.	Non-uniform magnetic fields from a magnetic dipole act on dual ferrofluid by inducing magnetisation.
Force on fluid	The Lorentz force is generated when an electric current interacts with a magnetic field.	Kelvin force results from magnetic field gradients acting on a magnetised fluid.
Magnetic field direction	Uniform.	Non-uniform (spatially varying at x and y directions).
Force direction	Perpendicular to fluid motion and magnetic field.	Along the magnetic field gradient.

Several studies have examined the influence of MHD effects on dual ferrofluid flow. A dual ferrofluid formulated from cobalt ferrite ($CoFe_2O_4$) and ferrite (Fe_3O_4) demonstrate improved heat transfer performance under MHD conditions relative to conventional ferrofluid [5]. Deebani *et al.,* [12] further extended this work [5] by incorporating MHD effects at an acute magnetic field angle along with thermal radiation. Hedayatnasab *et al.,* [13] reported that both nanoparticles possess strong magnetic response and long-term stability, these characteristics attributed to their high oxygen content. An increase in the magnetic parameter has been shown to elevate the local skin friction in a dual ferrofluid composed of $Fe_3O_4/CoFe_2O_4$ suspended in water [14]. Asghar *et al.,* [15] conducted research involving a MHD dual ferrofluid composed of $Fe_3O_4/CoFe_2O_4$ in water over a porous stretching and shrinking sheet. As the MHD effect parameter increases, the velocity profile increases while the temperature profile decreases. Anantha *et al.,* [16] and Nisar *et al.,* [17] have investigated the similar MHD dual ferrofluid, as in [5,12,15] which dissolved in a solution of 50%:50% ethylene glycol (EG) with water.

In the context of the FHD effect, Tahir *et al.,* [18] further demonstrated that a dual ferrofluid formulated from nickel-zinc ferrite ($NiZnFe_2O_4$) and manganese zinc ferrite ($MnZnFe_2O_4$) in kerosene and engine oil exhibited improved heat transfer performance under FHD conditions. Consequently, such a dual ferrofluid has been recommended for application in thermal management systems, including cooling and heating devices. Chuohan and Chaudhary [19] also reported that the fluid motion decays more rapidly under the influence of the FHD effect in a dual ferrofluid, $MnZnFe_2O_4/Fe_3O_4$. They also observed that the FHD effect induces heat generation within the fluid, resulting in a rise in the flow temperature. Recently, Magdy *et al.,* [20] reported that the FHD and MHD effects produce distinct flow patterns in unsteady ferrofluid flow.

Besides, the geometry of a solar collector plate plays a crucial role in determining its overall thermal performance, as it directly influences the way solar radiation is absorbed, distributed, and transferred to the working fluid. An inclined extending (or stretching) plate is a particularly significant geometric configuration in engineering applications, including solar collector systems, as illustrated in Figure 1. Moreover, the angle at which the sheet is inclined affects the gravitational force, which in turn changes the fluid flow due to the induced buoyancy force, thereby generating mixed convection in the fluid. Rani Titus and Abraham [21] investigated the impact of an inclination angle on a ferrofluid with the FHD effect. Their findings show that increasing the inclination angle reduces the velocity distribution associated with the FHD effect. They also reported that the inclination angle increases the thickness of the thermal boundary layer. Furthermore, Zainodin *et al.,* [22] discussed the behaviour of a $Fe_3O_4/CoFe_2O_4$ along an inclined porous stretching sheet with mixed convection parameter. This investigation revealed that the various values of inclination angle rapidly elevate the heat transfer rate and skin friction of the dual ferrofluid. Increasing the heat transfer rate is attributed to a greater buoyancy force when the sheet is altered from a horizontal to a vertical orientation. Azmi *et al*., [23] and Alabdulhadi *et al.,* [24] also concluded that the inclination parameter influences the behaviour of fluid flow by enhancing the fluid motion while reducing the temperature distribution.

Despite extensive research on ferrofluids, the literature reveals a significant gap, the coupled influence of FHD and MHD effects, inclination angle, and mixed convection on dual ferrofluid flow over an extending sheet remains largely unexplored. Moreover, to the best of the authors' knowledge, no existing study has investigated the behaviour of a dual ferrofluid composed of $Fe_3O_4/CoFe_2O_4$ nanoparticles dispersed in an ethylene glycol–water mixture under the simultaneous influence of both FHD and MHD effects. Motivated by the previous studies [19-21], the current research concentrates on the FHD and MHD effects on a mixed convection $Fe_3O_4/CoFe_2O_4 -$ 50% EG + 50% water dual ferrofluid flow across an inclined extending plate. The modified Tiwari and Das's model [25] has been applied to describe the thermophysical properties of

the dual ferrofluid flow. The governing equations in the form of partial differential equations (PDEs), including the continuity, momentum, and energy equations are developed. The complexity of the PDEs is reduced by introducing similarity variables, which transform the system into ordinary differential equations (ODEs). The resulting ODEs are subsequently solved using the bvp4c solver in MATLAB. The velocity and temperature profiles, as well as the surface shear stress and heat transfer rate, are subsequently analysed and presented graphically. The findings of this study are significant in providing new theoretical insight into the interaction of uniform and non-uniform magnetic fields, buoyancy forces, and surface inclination in dual ferrofluid flows, thereby offering useful guidance for the development and optimisation of magnetically controlled thermal and heat transfer systems. The objectives of this research are to investigate

i. the effects of uniform (MHD) and non-uniform (FHD) magnetic fields on a mixed convection dual ferrofluid flow,
ii. and the influences of inclination angle on dual ferrofluid over an extending plate.

2. Mathematical Formulation

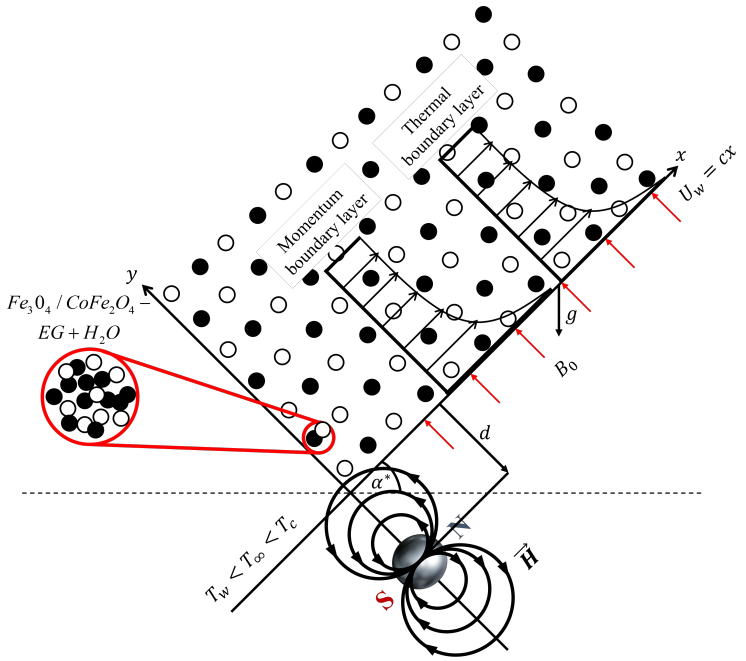

Fig. 2. Physical configuration of FHD and MHD effect over an inclined extending plate

The current study examines a steady, incompressible, two-dimensional, and laminar viscous dual ferrofluid flow over an inclined extending plate under the combined influences of FHD and MHD effects. The dual ferrofluid consists of ferrite (Fe_3O_4) and cobalt ferrite $(CoFe_2O_4)$ nanoparticles dispersed in a base fluid composed of 50% ethylene glycol (EG) and 50% water. The fluid motion is analysed in the (x, y) coordinate directions, where u and v denote the velocity components with respect to x and y, respectively. The plate extends along the x -axis with a stretching velocity $U_w = ax$, with $a > 0$ characterising the plate's stretching rate, as depicted in Figure 2 [12, 21]. The y-axis is taken to be normal to the sheet [18]. The plate is inclined at an angle α^*, which induces a buoyancy force within the fluid [21].

The surface of the plate is held at a uniform temperature T_w, whereas the ambient fluid temperature is denoted by T_∞. In the presence of magnetic nanoparticles, the system is additionally characterised by the Curie temperature T_c, which control their magnetic properties. The local

temperature of the dual ferrofluid is represented by T. Once the fluid temperature exceeds T_c, the nanoparticles can no longer sustain magnetisation. Accordingly, the temperature field in the present analysis is assumed to satisfy $T < T_w < T_\infty < T_c$ [18]. In modeling the FHD effect, a magnetic dipole is located below the x-axis, centered along the y-axis. The parameter d defines the vertical distance separating the dipole from the sheet. The magnetic moment is oriented in the positive x-direction (from the north pole toward the south pole), as illustrated in Figure 2, producing magnetic fields strong enough to magnetically saturate the dual ferrofluid [18]. Meanwhile, in the presence of the MHD effect, an external magnetic field B_0 is oriented perpendicular to the direction of fluid flow. The uniform MHD field and the non-uniform FHD field are assumed to act independently [20]. The induced magnetic field is neglected because it is small compared to the applied fields. Under this assumption, the total magnetic effect on the dual ferrofluid is treated as the sum of the two fields. The uniform MHD field produces a Lorentz force, while the non-uniform FHD field generates a Kelvin force. These forces affect the fluid simultaneously, but the magnetic fields themselves do not directly interact. Accordingly, the governing PDEs for the continuity, momentum, and energy equations may be written as [19-21]

$$\frac{\partial u}{\partial x} + \frac{\partial v}{\partial y} = 0, \tag{1}$$

$$\rho_{hff}\left(u\frac{\partial u}{\partial x} + v\frac{\partial u}{\partial y}\right) = M\mu_0\frac{\partial H}{\partial x} + \mu_{hff}\left(\frac{\partial^2 u}{\partial x^2} + \frac{\partial^2 u}{\partial y^2}\right) - \sigma_{hff}B_0^2 u + (\rho\beta^*)_{hff}(T_c - T)g\sin\alpha^*, \tag{2}$$

$$\begin{aligned}\left(\rho C_p\right)_{hff}\left(u\frac{\partial T}{\partial x} + v\frac{\partial T}{\partial y}\right) + \left(u\frac{\partial H}{\partial x} + v\frac{\partial H}{\partial y}\right)\mu_0 T\frac{\partial M}{\partial T} = k_{hff}\left(\frac{\partial^2 T}{\partial x^2} + \frac{\partial^2 T}{\partial y^2}\right)\\ +\mu_{hff}\left[2\left(\frac{\partial u}{\partial x}\right)^2 + 2\left(\frac{\partial v}{\partial y}\right)^2 + \left(\frac{\partial u}{\partial y} + \frac{\partial v}{\partial x}\right)^2\right].\end{aligned} \tag{3}$$

In Eq. (2), the term $M\mu_0\frac{\partial H}{\partial x}$ represents the magnetic body force per unit volume, where M denotes the magnetisation. This contribution is commonly known as the Kelvin force [26]. The terms $\frac{\partial H}{\partial x}$ and $\frac{\partial H}{\partial y}$ appearing in both Eqs. (2) and (3) denote the spatial gradient of the magnetic field strength in the x and y −directions, respectively. These gradients are expressed as [20]

$$\frac{\partial H}{\partial x} = -\frac{\gamma_1}{2\pi}\frac{2x}{(y+d)^4},$$

$$\frac{\partial H}{\partial y} = \frac{\gamma_1}{2\pi}\left(-\frac{2}{(y+d)^3} + \frac{4x^2}{(y+d)^5}\right).$$

The term $\frac{\partial M}{\partial T}$ in Eq. (3) represents the rate of change of magnetisation M with respect to temperature T. The magnetisation M is assumed to vary linearly with temperature and is given by [20]

$$M = K(T_c - T).$$

where K is the thermomagnetic coefficient, which characterises the influence of temperature gradients on the magnetic properties of the fluid. For the FHD effect to occur, the fluid temperature T must differ from the Curie temperature T_c, and the magnetic field must be non-uniform [26].

Eq. (2) captures the MHD effect, which arises due to the electrical conductivity σ_{hff} of the dual ferrofluid when subjected to the applied magnetic field B_0. The mixed convection term, expressed in the final part of Eq. (2), accounts for the combined influence of gravitational acceleration g and the

thermal expansion coefficient $(\rho\beta)^*$ [24]. The flat plate is inclined at an angle α^*, represented through $\sin\alpha^*$ [21]. Additionally, the final term in Eq. (3) indicates that viscous dissipation is caused by internal viscous shear in the dual ferrofluid.

The dual ferrofluid model Eqs. (1) to (3) are constrained by the following boundary conditions [18, 21]

$$y = 0:\ u - U_w = 0, v = 0, T = T_w, \tag{4}$$

$$y \to \infty:\ u = 0, T = T_c. \tag{5}$$

According to Eq. (4), the x-direction velocity fulfills the no-slip condition, meaning that the dual ferrofluid adheres to the plate and moves with the same velocity as the stretching surface. The velocity in the y-direction is initially zero. The dual ferrofluid temperature at the plate surface is T_w when $y = 0$. As the fluid moves away from the sheet toward the free stream ($y \to \infty$), the velocity approaches zero, and the temperature of the dual ferrofluid approaches the Curie temperature of the magnetic nanoparticles T_c [18] .

Table 2
Model of dual ferrofluid [5,12,22]

Properties	**Model**
Density	$\rho_{hff} = (1-\phi_{CoFe_2O_4})[\phi_{Fe_3O_4}\rho_{Fe_3O_4} + (1-\phi_{Fe_3O_4})\rho_{EG+water}] + \phi_{CoFe_2O_4}\rho_{CoFe_2O_4}$
Specified heat capacity	$(\rho C_p)_{hff} = (1-\phi_{CoFe_2O_4})\left[(1-\phi_{Fe_3O_4})(\rho C_p)_{EG+water} + \phi_{Fe_3O_4}(\rho C_p)_{Fe_3O_4}\right] + \phi_{CoFe_2O_4}(\rho C_p)_{CoFe_2O_4}$
Thermal expansion coefficient	$(\rho\beta^*)_{hff} = \phi_{CoFe_2O_4}(\rho\beta^*)_{CoFe_2O_4} + (1-\phi_{CoFe_2O_4})[\phi_{Fe_3O_4}(\rho\beta^*)_{Fe_3O_4} + (1-\phi_{Fe_3O_4})(\rho\beta^*)_{EG+water}] +$
Dynamic viscosity	$\mu_{hff} = \frac{\mu_{EG+water}}{(1-\phi_{Fe_3O_4})^{2.5}(1-\phi_{CoFe_2O_4})^{2.5}}$
Thermal conductivity	$k_{hff} = \frac{k_{CoFe_2O_4} + 2k_{Fe_3O_4} - 2\phi_{CoFe_2O_4}(k_{Fe_3O_4} - k_{CoFe_2O_4})}{k_{CoFe_2O_4} + 2k_{Fe_3O_4} + \phi_{CoFe_2O_4}(k_{Fe_3O_4} - k_{CoFe_2O_4})} \times k_{Fe_3O_4}$
where	$\frac{k_{Fe_3O_4}}{k_{EG+water}} = \frac{k_{Fe_3O_4} + 2k_{EG+water} - 2\phi_{CoFe_2O_4}(k_{EG+water} - k_{Fe_3O_4})}{k_{Fe_3O_4} + 2k_{EG+water} + \phi_{CoFe_2O_4}(k_{EG+water} - k_{Fe_3O_4})}$,
Electrical conductivity	$\sigma_{hff} = \frac{\sigma_{CoFe_2O_4} + 2\sigma_{Fe_3O_4} - 2\phi_{CoFe_2O_4}(\sigma_{Fe_3O_4} - \sigma_{CoFe_2O_4})}{\sigma_{CoFe_2O_4} + 2\sigma_{Fe_3O_4} + \phi_{CoFe_2O_4}(\sigma_{Fe_3O_4} - \sigma_{CoFe_2O_4})} \times \sigma_{Fe_3O_4}$
where	$\frac{\sigma_{Fe_3O_4}}{\sigma_{EG+water}} = \frac{\sigma_{Fe_3O_4} + 2\sigma_{EG+water} - 2\phi_{CoFe_2O_4}(\sigma_{EG+water} - \sigma_{Fe_3O_4})}{\sigma_{Fe_3O_4} + 2\sigma_{EG+water} + \phi_{CoFe_2O_4}(\sigma_{EG+water} - \sigma_{Fe_3O_4})}$

The dual ferrofluid coefficients established in Eqs. (2) and (3) pertain to the modification of the nanofluid model proposed by Tiwari and Das [25] are summarised in Table 2 [5,12,22]. The values of the thermophysical properties for Fe_3O_4 and $CoFe_2O_4$ nanoparticles together with the conventional fluid of mixture EG-water are presented in Table 3 [16,17].

Table 3
The thermophysical traits of dual ferrofluid [16,17]

Properties	Fe_3O_4	$CoFe_2O_4$	Ethylene glycol with water (50%:50%)
$\rho(kgm^{-3})$	5180	4907	1056
$C_p(Jkg^{-1}K^{-1})$	670	700	3.288
$k(Wm^{-1}K^{-1})$	9.7	3.7	0.425
$\beta \times 10^{-5}(K^{-1})$	0.5	1.3	0.00341
$\sigma\ (Sm^{-1})$	0.74×10^6	1.1×10^7	0.00509
Pr	-	-	29.86

2.1 Similarity Variables

Using the following similarity variables, [21]

$$\psi(\xi,\eta) = \nu_f \xi f(\eta), \qquad (\xi,\eta) = \left(\left(\frac{c}{\nu_f}\right)^{\frac{1}{2}} x, \left(\frac{c}{\nu_f}\right)^{\frac{1}{2}} y\right), \qquad \theta(\xi,\eta) = \frac{T_c - T}{T_c - T_w} = \theta_1(\eta) + \xi^2\theta_2(\eta), \tag{6}$$

the system of coupled PDEs with boundary conditions, (1) to (5) is reduced to ODEs. Here, $f(\eta)$ is the similarity function, $\nu_f = \frac{\mu}{\rho}$ is the kinematic viscosity, $\psi(\xi,\eta)$ is the stream function, and $\theta(\xi,\eta)$ is the dimensionless temperature both depending on the independent variables (ξ,η). The stream function $\psi(\xi,\eta)$ automatically satisfies the continuity Eq. (1), and the velocity components of the dual ferrofluid flow are expressed as $v = -\frac{\partial\psi}{\partial x} = -\sqrt{c\mu/\rho}\, f(\eta)$ in the y-direction, and $u = \frac{\partial\psi}{\partial y} = cxf'(\eta)$ in the x-direction. By imposing Eq. (6) into Eqs. (2) and (3), yields

$$f''' - \left(\frac{\rho_{hff}}{\rho_{cf}}\right)\left(\frac{\mu_{cf}}{\mu_{hff}}\right)[(-f'^2 + ff'')] - 2\left(\frac{\mu_{cf}}{\mu_{hff}}\right)\frac{\beta\theta_1}{(\eta+\alpha)^4} - \left(\frac{\sigma_{hff}}{\sigma_{cf}}\right)\left(\frac{\mu_{cf}}{\mu_{hff}}\right)B_0^2 Mf' + \left(\frac{\rho_{hff}}{\rho_{bf}}\right)\left(\frac{(\rho\beta^*)_{hff}}{(\rho\beta^*)_{cf}}\right)\lambda\theta_1 \sin\alpha^* = 0, \tag{7}$$

$$\left(\frac{k_{hff}}{k_{cf}}\right)(\theta_1'' + 2\theta_2) + \left(\frac{(\rho C_p)_{hff}}{(\rho C_p)_{cf}}\right)Prf\theta_1' + \frac{2\chi\beta f(\theta_1 - \varepsilon)}{(\eta+\alpha)^3} - \left(\frac{\mu_{hff}}{\mu_{cf}}\right)4\chi f'^2 = 0, \tag{8}$$

$$\left(\frac{k_{hff}}{k_{cf}}\right)\theta_2'' - \left(\frac{(\rho C_p)_{hff}}{(\rho C_p)_{cf}}\right)Pr(2f'\theta_2 - f\theta_2') - \lambda\beta(\theta_1 - \varepsilon)\left[\frac{2f'}{(\eta+\alpha)^4} + \frac{4f}{(\eta+\alpha)^5}\right] + \frac{2\chi\beta f\theta_2}{(\eta+\alpha)^3} - \left(\frac{\mu_{hff}}{\mu_{cf}}\right)\chi f''^2 = 0. \tag{9}$$

The boundary conditions (4) and (5) are reduced to

$$\text{at } \eta = 0: f(\eta) = 0, f'(\eta) = 1, \theta_1(\eta) = 1, \theta_2(\eta) = 0, \tag{10}$$

$$\text{at } \eta \to \infty: f'(\eta) \to 0, \theta_1(\eta) \to 0, \theta_2(\eta) \to 0. \tag{11}$$

Here, the prime (′) denotes differentiation with respect to η. The dimensionless parameters used in Eqs. (7) to (9) are defined as follows.

$Pr = \frac{\mu C_\rho}{k}$: Prandtl number, $\chi = \frac{c\mu^2}{\rho k(T_c - T_w)}$: Viscous dissipation,

$\varepsilon = \frac{T_c}{T_c - T_w}$: Curie temperature, $\beta = \frac{\gamma}{2\pi}\frac{\mu_0 K(T_c - T_w)\rho}{\mu^2}$: FHD effect,

$\alpha = \sqrt{\frac{c\rho}{\mu}}d$: Dimensionless distance, $M = \frac{\sigma_{cf}}{a\rho_{cf}}B_0^2$: MHD effect,

$\lambda = \frac{Gr_x}{Re_x^2} = \frac{\left[\frac{g\beta^*(T_c - T)}{c^2 x}\right]}{Re_x^2} = \frac{g\beta^*(T_c - T)x^3}{{\nu_f}^2}$: Mixed convection parameter.

2.2 Physical Quantities

The local skin friction C_f, is defined in terms of the wall shear stress, τ_w [18, 21]

$$C_f = -\frac{2\tau_w}{\rho_{cf}U_w^2}, \text{where } \tau_w = \mu_{hff}\left.\frac{\partial u}{\partial y}\right|_{y=0}.$$

The Nusselt number Nu_x, representing the heat transfer rate q_w, is expressed as [18, 21]

$$Nu_x = \frac{xq_w}{k_{cf}(T_c - T_w)}, \text{where } q_w = -k_{hff}\left.\frac{\partial T}{\partial y}\right|_{y=0}.$$

Using the similarity transformations (13) and the Reynolds number $Re = U_w\left(\frac{x}{\nu_f}\right)$, the dimensionless forms of C_f and $\mathrm{Nu}_x$are obtained as [18, 21]

$$C_f Re_x^{\frac{1}{2}} = -\frac{2}{\left(1-\varphi_{Fe_3O_4}\right)^{2.5}\left(1-\varphi_{CoFe_2O_4}\right)^{2.5}}f''(0) \text{ and}$$

$$Nu_x Re_x^{-\frac{1}{2}} = -\frac{k_{Fe_3O_4/CoFe_2O_4-\mathrm{EG+water}}}{k_{\mathrm{EG+water}}}[\theta_1'(0) + \xi^2\theta_2'(0)].$$

3. Numerical Method

The transformed system of ODEs (7) to (9) along with the boundary conditions (10) to (11) is solved numerically using the MATLAB bvp4c solver. This solver employs a collocation method to approximate the solution of boundary value problems for ODEs [27]. To implement the numerical method, the higher-order ODEs are first transformed into a system of first-order equations by introducing the following new dependent variables

$$f(\eta) = y(1), f'(\eta) = y(2), f''(\eta) = y(3), \theta_1 = y(4), \theta_1' = y(5), \theta_2 = y(6), \theta_1' = y(7). \quad (12)$$

Substituting Eq. (12) into Eqs. (7) to (9) yields the following system of first-order differential equations

$$y(3)' - \left(\frac{\rho_{hff}}{\rho_{cf}}\right)\left(\frac{\mu_{cf}}{\mu_{hff}}\right)\left[\left(-y(2)^2 + y(1)v(3)\right)\right] - 2\left(\frac{\mu_{cf}}{\mu_{hff}}\right)\frac{\beta y(4)}{(\eta+\alpha)^4} - \left(\frac{\sigma_{hff}}{\sigma_{cf}}\right)\left(\frac{\mu_{cf}}{\mu_{hff}}\right)B_0^2 M y(2) + \left(\frac{\rho_{hff}}{\rho_{bf}}\right)\left(\frac{(\rho\beta^*)_{hff}}{(\rho\beta^*)_{cf}}\right)\lambda y(4)\sin\alpha^* = 0, \tag{13}$$

$$\left(\frac{k_{hff}}{k_{cf}}\right)\left(y(5)' + 2y(6)\right) + \left(\frac{\left(\rho C_p\right)_{hff}}{\left(\rho C_p\right)_{cf}}\right)Pry(1)y(5) + \frac{2\chi\beta y(1)(y(4)-\varepsilon)}{(\eta+\alpha)^3} - \left(\frac{\mu_{hff}}{\mu_{cf}}\right)4\chi y(2)^2 = 0, \tag{14}$$

$$\left(\frac{k_{hff}}{k_{cf}}\right)y(7)' - \left(\frac{\left(\rho C_p\right)_{hff}}{\left(\rho C_p\right)_{cf}}\right)Pr\left(2y(2)y(6) - y(1)y(7)\right) + \frac{2\chi\beta y(1)y(6)}{(\eta+\alpha)^3} - \lambda\beta(y(4)-\varepsilon)\left[\frac{2y(2)}{(\eta+\alpha)^4} + \frac{4y(1)}{(\eta+\alpha)^5}\right] - \left(\frac{\mu_{hff}}{\mu_{cf}}\right)\chi y(2)^3 = 0. \tag{15}$$

The corresponding boundary conditions (10) and (11) expressed in terms of the first-order variables are

$$\text{at } y_a: y_a(1) = 0, y_a(2) = 1, y_a(4) = 1, y_a(6) = 0, \tag{16}$$

$$\text{at } y_b: y_b(2) \to 0, y_b(4) \to 0, y_b(6) \to 0. \tag{17}$$

An initial guess for the solution over the computational domain is provided, which serves as a starting point for the solver. The initial guesses that satisfy the boundary conditions (10) and (11) are selected as

$$f(\eta) = 1 - e^{-\eta}, \theta_1(\eta) = e^{-\eta}, \theta_2(\eta) = \eta e^{-\eta}\ .$$

The `bvp4c` algorithm iteratively refines this guess to satisfy both the ODEs system and the boundary conditions simultaneously [27]. The bvp4c solution procedure is illustrated in Figure 3

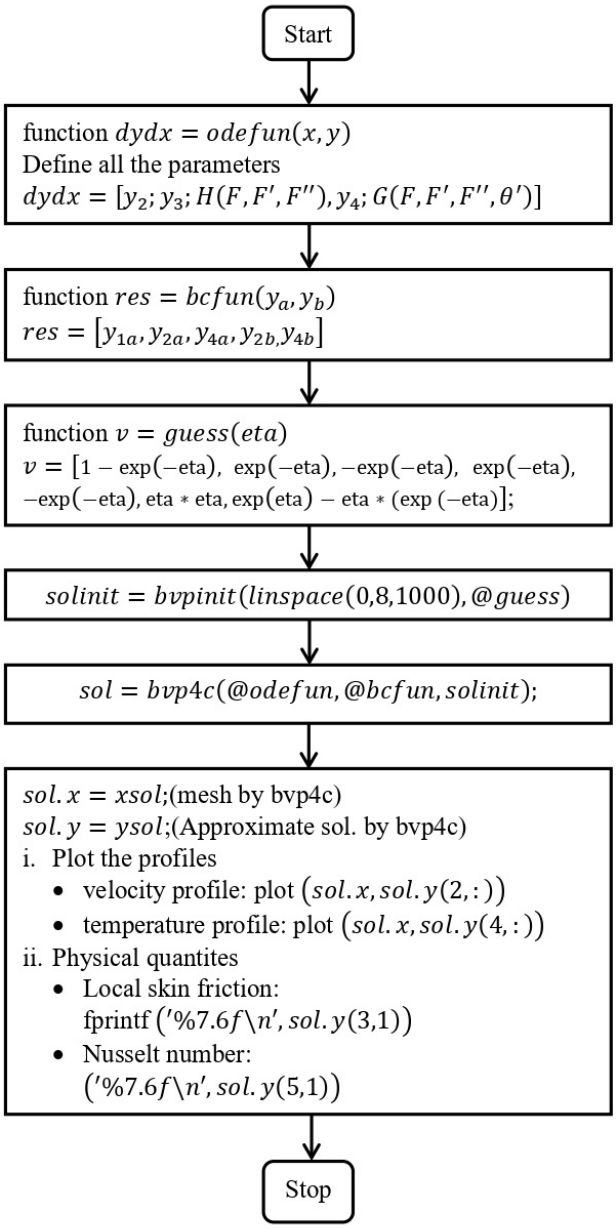

Fig. 3. Flowchart for bvp4c

4. Results and Discussion

The main objective of the present study is to examine the effects of MHD and FHD on the behaviour of a dual ferrofluid flowing over an inclined extending plate. The Prandtl number of $\text{Pr} = 29.86$ corresponds to the thermophysical properties of the base fluid consisting of 50% EG and 50% water (see Table 3). The dimensionless parameter $\alpha = 1.0$ represents the relative position of the magnetic dipole beneath the plate, chosen to be on the same order as the boundary layer thickness. The parameter $\epsilon = 2.0$ denotes the temperature ratio between the surface temperature of the plate and the Curie temperature of the magnetic nanoparticles, applicable in the region far from the boundary layer. The dimensionless parameter $\chi = 0.01$ accounts for viscous heat dissipation arising from fluid viscosity [26]. The range of investigated parameters are $1 \leq \beta \leq 4$ [19], $1 \leq M \leq 4$ [16]

and $0 \leq \alpha^* \leq \frac{\pi}{2}$ [21]. In this study, the FHD effect is examined by considering the parameter $\beta$with $M = 0$, whereas the MHD effect is examined by considering the parameter M with $\beta = 0$.

4.1 Validation

For validation, the present study is compared with an established case from the literature. Table 4 provides the comparative values of $Nu_x Re_x^{-1/2}$for various Pr when $\beta = M = \alpha = \epsilon = \chi = \phi_1 = \phi_2 = \alpha^* = 0$. The numerical results exhibit excellent agreement with the existing solutions reported by Chouhan and Chaudhary [19], as demonstrated in Table 4. This strong consistency verifies the accuracy of the present computations, allowing the numerical method to be confidently applied to analyse the remaining aspects of the problem.

Table 4
Results validation for $Nu_x Re_x^{-1/2}$ for parameters Pr

Pr	Chouhan and Chaudhary [19]	Present study
0.70	0.4540	0.4538
2.00	0.9113	0.9112
3.00	1.1653	1.1651
7.00	1.8954	1.8953
10.0	2.3080	2.3079
20.0	3.3539	3.3539
70.0	6.4622	6.4622

4.2 Velocity and Temperature Profiles

Figure 4 presents the effects of uniform and non-uniform magnetic fields on the velocity profile $f'(\eta)$. The MHD effect is associated with a uniform magnetic field and is quantified by the parameter M, whereas the FHD effect is associated with a non-uniform magnetic field and is quantified by the parameter β. From Figure 4, the blue dotted curve ($M = \beta = 0$) describes the flow without the magnetic field effect. Therefore, yields the highest velocity values and the thickest boundary layer. In this condition, the motion of the fluid is controlled only by viscous forces without any additional magnetic field influence.

In the presence of a uniform magnetic field, higher values of the magnetic parameter M cause a noticeable decrease in the profile $f'(\eta)$, as the resulting Lorentz force acts against the fluid motion. This results in a more pronounced deceleration and a noticeably thinner boundary layer. In contrast, increasing the non-uniform magnetic parameter β also reduces the profile of $f'(\eta)$, but the effect is comparatively weaker because the induced Kelvin force varies spatially and is less dominant than in the uniform case. Consequently, all magnetic field cases lie below the no-field case ($M = \beta = 0$) profile, with the uniform magnetic field (MHD) producing the faster reduction of velocity, while the non-uniform magnetic field (FHD) yields a more moderate reduction.

For solar collector plate applications, these results show that the magnetic fields can control the speed of the fluid moving over the heated plate, which may enhance heat absorption by allowing the fluid to stay longer near the surface. From Figure 4, it can be stated that the MHD effect has the potential to improve the efficiency of a solar collector plate by controlling fluid motion near the heated surface.

The relationship between the magnetic fields effect and the temperature profile $\theta_1(\eta)$ is illustrated in Figure 5. The results clearly show that the temperature of the dual ferrofluid increases when the magnetic fields parameters M and β increase from the baseline case $M = \beta = 0$. This

temperature rise is attributed to the reduction of fluid motion, as indicated by the deceleration of the velocity gradient $f'(\eta)$. When M and β are nonzero, the thinner momentum boundary leads to higher heat transfer from the plate to the fluid, which weakens convective cooling. Thus, the thermal boundary layer thickness increases from without magnetic fields to with magnetic fields.

Moreover, the increase in the profile $\theta_1(\eta)$ is more pronounced under the influence of the MHD effect as the parameter M increases. This demonstrates that the MHD effect causes greater energy dissipation compared to the FHD effect. Overall, the results show that a stronger MHD effect increases the temperature of the dual ferrofluid more effectively than the FHD effect. This is useful for solar collector plates because a higher fluid temperature helps the system absorb and store more heat.

The influence of the inclined angle parameter α^* for the profile of $f'(\eta)$ is displayed in Figure 6 for both cases of non-uniform $(\beta = 3)$ and uniform $(M = 3)$ magnetic fields. Increasing the parameter α^* from 0 to $\frac{\pi}{2}$ leads to enhancing the profile of $f'(\eta)$. Physically, the component of the gravitational force along the surface increases as the parameter α^*rises, resulting in a larger pressure gradient along the surface.

When $\alpha^* = 0$, the sheet is horizontal, and the buoyancy force in the dual ferrofluid is relatively weak. As α^*varies from 0 to $\frac{\pi}{2}$, the sheet gradually becomes vertical, and the buoyancy force reaches its maximum. Consequently, the strength of buoyancy forces in the dual ferrofluid enhances natural convection proportionally to $\sin\alpha^*$. This leads to more vigorous fluid motion, allowing fluid particles to move more freely and increasing the thickness of the momentum boundary layer.

Among the two magnetic configurations, the highest $f'(\eta)$ is observed under the non-uniform FHD effect $(\beta = 3)$, indicating that non-uniform magnetic fields promote stronger fluid acceleration compared to the uniform MHD case $(M = 3)$. This is because a non-uniform magnetic field creates spatial variations in magnetic force**.** These variations act like an additional driving force that pushes and accelerates the fluid more strongly**.**

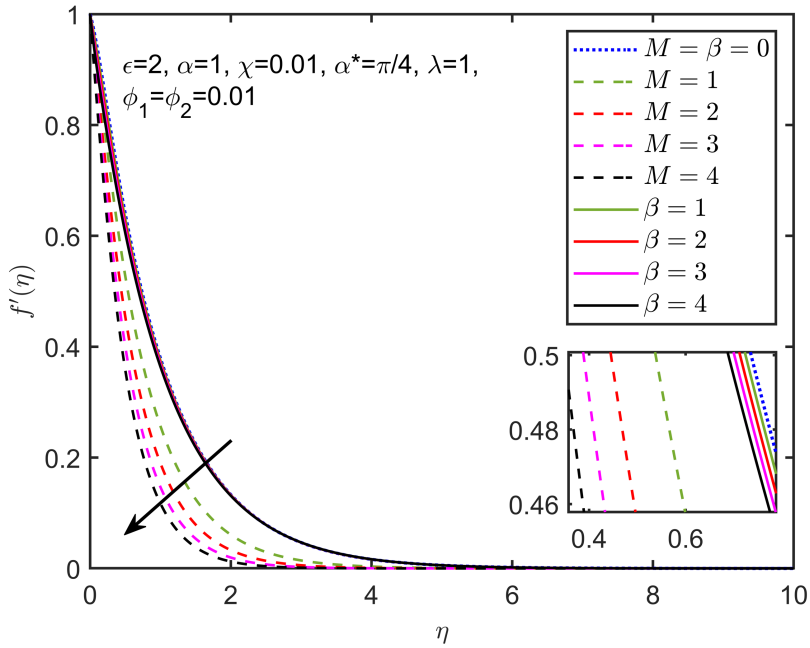

Fig. 4. Influences of uniform (M) and non-uniform (β) magnetic fields on $f'(\eta)$

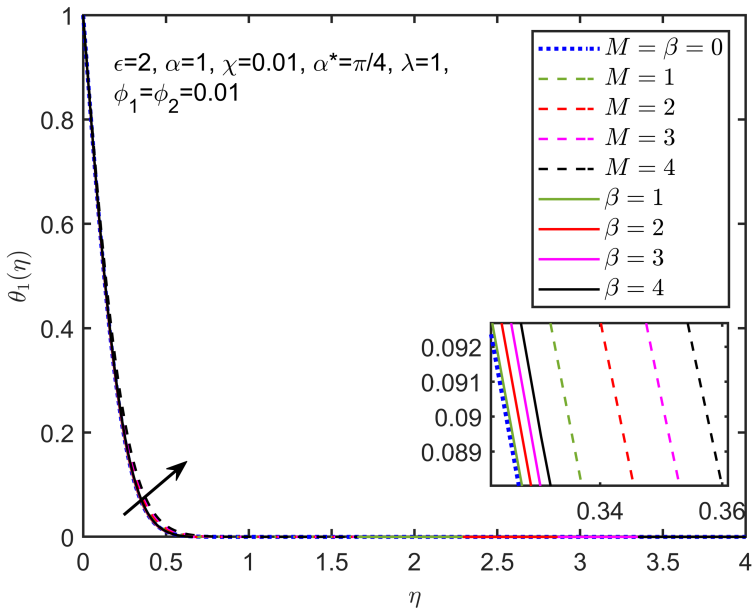

Fig. 5. Influences of uniform (M) and non-uniform (β) magnetic fields on $\theta_1(\eta)$

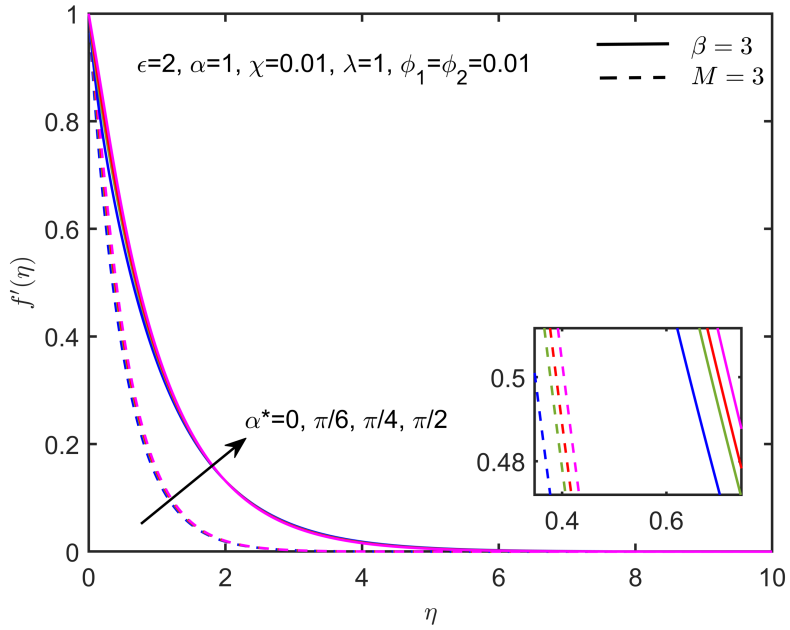

Fig. 6 Influences of the parameter α^* for the cases of $(\beta = 3)$ and $(M = 3)$ on $f'(\eta)$

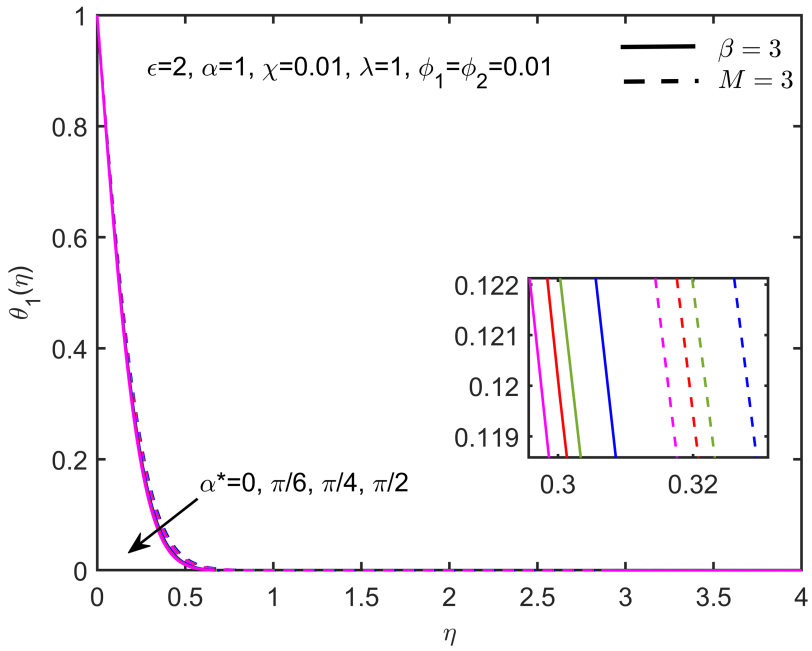

Fig. 7. Influences of the parameter α^* for the cases of $(\beta = 3)$ and $(M = 3)$ on $\theta_1(\eta)$

Figure 7 shows the behaviour of $\theta_1(\eta)$ as the parameter α^* is increased. It is observed that the distribution of θ_1 decreases when the sheet inclination changes from $\alpha^* = 0$ to $\alpha^* = \frac{\pi}{2}$. The increase in the profile of $f'(\eta)$ enhances the tendency of the fluid to transfer heat via convection while reducing heat conduction between the fluid and the wall. As a result, the fluid temperature near the sheet decreases, and the thermal boundary layer becomes thinner.

The reduction in $\theta_1$is more pronounced for the case $\beta = 3$ compared to $M = 3$. This is because the uniform magnetic field case $(M = 3)$ produces a thinner momentum boundary layer, which enhances heat transfer to the fluid from the plate. For a solar collector plate, these results show that increasing the inclination angle improves natural convection along the plate surface. This causes stronger fluid motion and better cooling of the plate. The non-uniform magnetic configuration with $\beta = 3$ increases this effect by producing greater fluid acceleration and heat removal. As a result, the plate reaches a lower surface temperature and achieves better thermal performance, which is important for efficient solar energy absorption and stable operation.

4.3 Surface Shear Stress and Heat Transfer Rate

The effect of parameters α^* and β on the characteristics of $C_f Re_x^{1/2}$ is presented in Figure 8. It is demonstrated that an increase in the parameter α^* diminishes the behaviour of $C_f Re_x^{1/2}$. This is because the buoyancy force reduces the frictional force between the fluid and the wall of the sheet, allowing the fluid to flow more freely under the dominance of the buoyancy force. As a result, the shear stress decreases. However, Figure 8 shows that the behaviour of $C_f Re_x^{1/2}$ increases with the values of parameter β. This trend is attributed to the reduction in the velocity gradient profile $f'(\eta)$, which reflects greater resistance of the fluid to flow freely. The existence of the FHD effect has increased the surface shear stress.

Figure 9 depicts the relationship between the parameter α^* and the values of $Nu_x Re_x^{-1/2}$. It is perceived that an augment in the parameter α^* increases the values of $Nu_x Re_x^{-1/2}$. This is attributed

to the enhancement of the convective heat transfer rate compared to the conductive heat transfer rate in the dual ferrofluid as the fluid flows faster. As a result, the values of $Nu_x Re_x^{-1/2}$ increase with an increase in the parameter α^*. A reduction in the values of $Nu_x Re_x^{-1/2}$ is observed with increasing values of the parameter β, indicating a decline in heat transfer efficiency under stronger FHD effect. This is due to the deceleration of $f'(\eta)$, resulting in more heat being transferred to the sheet through conduction rather than convection. As a result, the heat transfer coefficient rapidly reduces when the parameter β increases.

Figure 10 exhibits the effect of parameter λ on the values of $C_f Re_x^{1/2}$. It is observed that the values of $C_f Re_x^{1/2}$ reduce as the parameter λ increases. This behaviour is attributed to the buoyancy force, which increases fluid motion and reduces wall shear stress. However, increasing the parameter M results in a rise in $C_f Re_x^{1/2}$. This occurs because the stronger magnetic fields reduce the velocity gradient $f'(\eta)$, leading to an increase in surface shear stress at the plate.

The relationship between the parameter λ and the values of $Nu_x Re_x^{-1/2}$ is displayed in Figure 11. The values of $Nu_x Re_x^{-1/2}$ increase with the rise in the parameter λ, attributed to the increase in the profile of $f'(\eta)$. This indicates that convective heat transfer dominates over conductive heat transfer. However, the values of $Nu_x Re_x^{-1/2}$ decrease with increasing parameter M. This occurs because the magnetic fields reduce the profile $f'(\eta)$, which weakens convection and allows conduction to dominate.

These results show that parameters that strengthen fluid motion, such as the parameters $\alpha^*$and λ, improve convective heat transfer and help the dual ferrofluid absorb heat more efficiently from a solar collector plate. In contrast, MHD and FHD effects (M and β) slow the fluid, increase shear stress, and reduce heat transfer. Therefore, enhancing buoyancy-driven flow while controlling magnetic influence can improve the overall thermal performance of solar collector plates using dual ferrofluid.

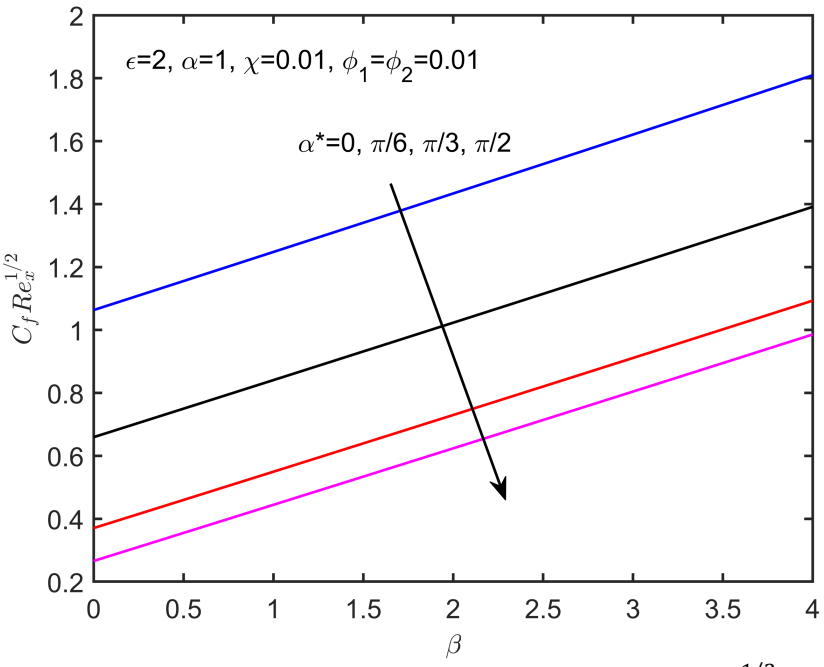

Fig. 8. Influences of the parameters α^* and β on $C_f Re_x^{1/2}$

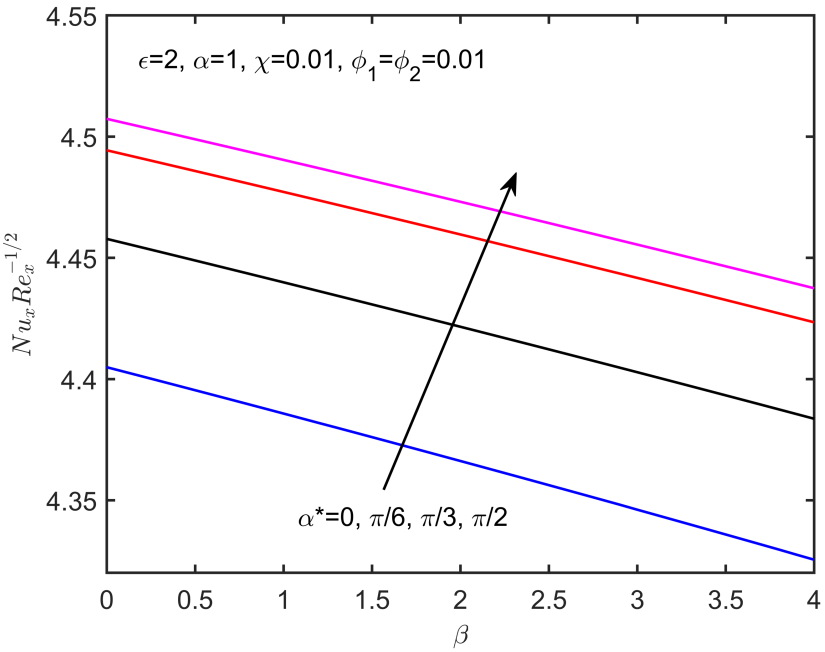

Fig. 9. Influences of the parameters α^* and β on $Nu_x Re_x^{-1/2}$

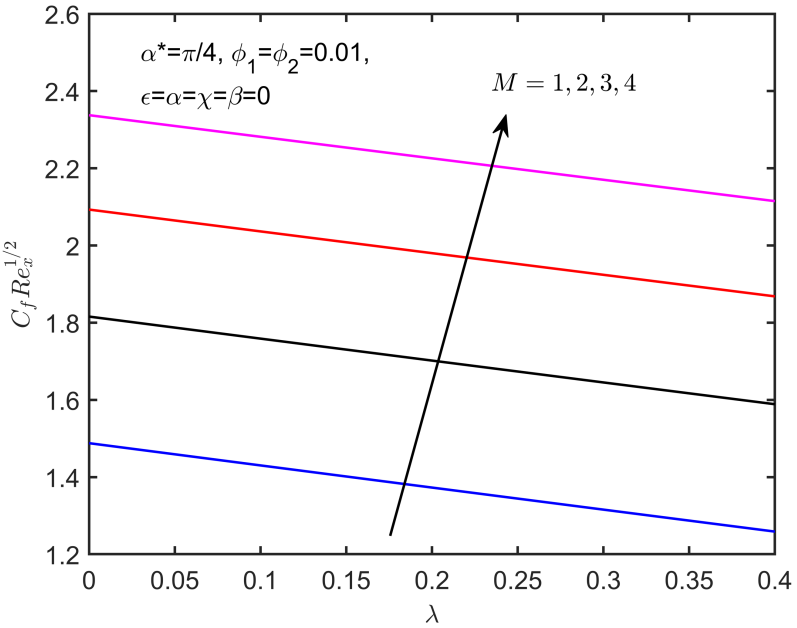

Fig. 10. Influences of the parameters λ and M on $C_f Re_x^{1/2}$

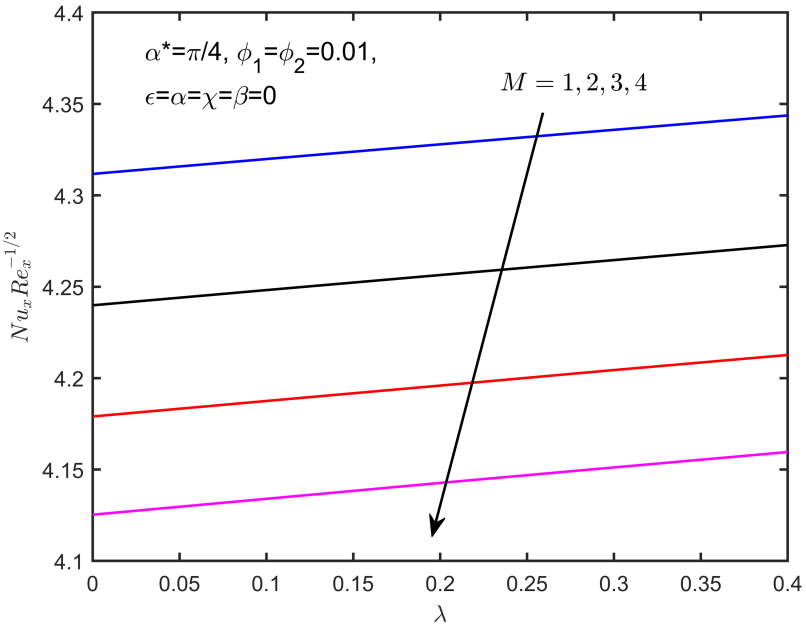

Fig. 11. Influences of the parameters λ and M on $Nu_x Re_x^{-1/2}$

5. Conclusion

In this study, the influence of both uniform and non-uniform magnetic fields on a dual ferrofluid comprising ferrite (Fe_3O_4), and cobalt ferrite $(CoFe_2O_4)$ nanoparticles in an equal ethylene glycol-water mixture over an inclined extending plate. The uniform and non-uniform magnetic fields are represented by the MHD and FHD effects, respectively. The governing model is formulated using partial differential equations (PDEs), which are then simplified through a similarity transformation to obtain a system of ordinary differential equations (ODEs). These equations are solved numerically using the bvp4c solver in MATLAB. The analysis focuses on the effects of the MHD effect M, FHD effect β, inclination angle α^* and mixed convection parameter λ on the behaviour of the dual ferrofluid. Detailed results are presented for the velocity profile $f'(\eta)$ and temperature profile $\theta_1(\eta)$, and the related physical quantities, namely the surface shear stress $C_f Re_x^{1/2}$ and the heat transfer rate $Nu_x Re_x^{-1/2}$. The key findings are summarised as follows.

i. The presence of magnetic fields causes a faster reduction in the profile of $f'(\eta)$ with the MHD parameter M producing the strongest decelerating effect.
ii. The temperature of the dual ferrofluid increases more noticeably when the MHD parameter M becomes larger compared to the FHD parameter β.
iii. Increasing the inclination angle α^* enhances the profile $f'(\eta)$ but an opposite trend occurs for the profile $\theta_1(\eta)$.
iv. The values of C_f $\mathrm{Re}_x^{1/2}$ decreases as the parameters α^* and λ increase. In contrast, the values of Nu_x $\mathrm{Re}_x^{-1/2}$ increases with both parameters.
v. When the magnetic parameters M and β increase, the values of C_f $\mathrm{Re}_x^{1/2}$ also increases, while the values of Nu_x $\mathrm{Re}_x^{-1/2}$ decreases.

The results of this study highlight the importance of considering magnetic effects (uniform and non-uniform), inclination angle, and mixed convection when designing a solar collector plate that

uses dual ferrofluid for thermal enhancement. Each parameter plays a distinct role in controlling fluid motion, temperature distribution, and overall heat transfer performance.

Future work may incorporate additional physical mechanisms, particularly thermal radiation [6] and velocity slip [15] effects, to further improve the accuracy of the model. Considering thermal radiation is important because solar collector plates operate at elevated temperatures, where radiative heat transfer becomes comparable to convection and significantly influences the overall thermal efficiency. Including radiation in the analysis would allow a more realistic prediction of heat losses from the absorber surface under strong solar exposure. In addition, accounting for velocity slip at the wall is relevant for dual ferrofluid used in practical solar thermal systems. The presence of nanoparticles and surface coatings on absorber plates can induce partial slip, which alters the near-wall velocity, shear stress, and heat transfer characteristics. Incorporating slip effects into future models would therefore provide a more accurate representation of the actual flow behaviour inside solar collector plate.

Acknowledgement
This work was supported by the Universiti Teknologi Malaysia under UTM Fundamental Research Grant Vote No: Q.J130000.3854.23H22.

References

[1] Ehsan Shojaeizadeh, Farzad Veysi, Kourosh Zareinia, and Amir Mohammad Mansouri. "Thermal efficiency of a ferrofluid-based flat-plate solar collector under the effect of non-uniform magnetic field." *Applied Thermal Engineering* 201 (2022): 117726. https://doi.org/10.1016/j.applthermaleng.2021.117726

[2] Siddharth Suman, Mohd Kaleem Khan, and Manabendra Pathak. "Performance enhancement of solar collectors—A review." *Renewable and Sustainable Energy Reviews* 49 (2015): 192-210. https://doi.org/10.1016/j.rser.2015.04.087

[3] Arun Kumar Tiwari. "Application of nanoparticles in solar collectors: a review." *Materials Today: Proceedings* 2, no. 4-5 (2015): 3638-3647. https://doi.org/10.1016/j.matpr.2015.07.121

[4] Gary J O'Keeffe, *Mathematical modelling of nanofluid-based direct absorption solar collectors*. 2018, University of Limerick. https://doi.org/10.1016/j.solener.2018.08.073

[5] Sakinah Idris, Anuar Jamaludin, Roslinda Nazar, and Ioan Pop. "Heat transfer characteristics of magnetized hybrid ferrofluid flow over a permeable moving surface with viscous dissipation effect." *Heliyon* 9, no. 5 (2023): https://doi.org/10.1016/j.heliyon.2023.e15907

[6] Bagh Ali, Imran Siddique, Ilyas Khan, Bilal Masood, and Sajjad Hussain. "Magnetic dipole and thermal radiation effects on hybrid base micropolar CNTs flow over a stretching sheet: Finite element method approach." *Results in Physics* 25 (2021): 104145. https://doi.org/10.1016/j.rinp.2021.104145

[7] Sajjad Sarvar, Saman Rashidi, and Roohollah Rafee. "A brief review of the application of ferrofluids and magnetic fields in solar energy systems." *Journal of Magnetism and Magnetic Materials* 588 (2023): 171435. https://doi.org/10.1016/j.jmmm.2023.171435

[8] BA Finlayson. "Convective instability of ferromagnetic fluids." *Journal of Fluid Mechanics* 40, no. 4 (1970): 753-767. https://doi.org/10.1017/S0022112070000423

[9] Joanna Dulińska-Litewka, Agnieszka Łazarczyk, Przemysław Hałubiec, Oskar Szafrański, Karolina Karnas, and Anna Karewicz. "Superparamagnetic iron oxide nanoparticles—Current and prospective medical applications." *Materials* 12, no. 4 (2019): 617. https://doi.org/10.3390/ma12040617

[10] RE Rosensweig. "Directions in ferrohydrodynamics." *Journal of Applied Physics* 57, no. 8 (1985): 4259-4264. https://doi.org/10.1063/1.334579

[11] René J Moreau, *Magnetohydrodynamics*. Vol. 3. 2013: Springer Science & Business Media.

[12] Wejdan Deebani, Ubaidullah Yashkun, Sumera Dero, Liaquat Ali Lund, Zahir Shah, Narcisa Vrinceanu, and Meshal Shutaywi. "Numerical simulation and stability analysis of Radiative magnetized hybridized

ferrofluid flow with acute magnetic force over shrinking/stretching surface." *Results in Engineering* (2024): 102315. https://doi.org/10.1016/j.rineng.2024.102315

[13] Ziba Hedayatnasab, Faisal Abnisa, and Wan Mohd Ashri Wan Daud. "Review on magnetic nanoparticles for magnetic nanofluid hyperthermia application." *Materials & Design* 123 (2017): 174-196. https://doi.org/10.1016/j.matdes.2017.03.036

[14] Najiyah Safwa Khashi'Ie, Iskandar Waini, Nur Syahirah Wahid, Norihan Md Arifin, and Ioan Pop. "Radiative hybrid ferrofluid flow over a permeable shrinking sheet in a three-dimensional system." *CFD Letters* 14 (2022): 9-21. https://doi.org/10.37934/cfdl.14.11.921

[15] Adnan Asghar, Sumera Dero, Liaquat Ali Lund, Zahir Shah, Mansoor H Alshehri, and Narcisa Vrinceanu. "Slip effects on magnetized radiatively hybridized ferrofluid flow with acute magnetic force over shrinking/stretching surface." *Open Physics* 22, no. 1 (2024): 20240052. https://doi.org/10.1515/phys-2024-0052

[16] K Anantha Kumar, N Sandeep, V Sugunamma, and IL Animasaun. "Effect of irregular heat source/sink on the radiative thin film flow of MHD hybrid ferrofluid." *Journal of Thermal Analysis and Calorimetry* 139 (2020): 2145-2153. https://doi.org/10.1007/s10973-019-08628-4

[17] Kottakkaran Sooppy Nisar, Umair Khan, A Zaib, Ilyas Khan, and Dumitru Baleanu. "Numerical simulation of mixed convection squeezing flow of a hybrid nanofluid containing magnetized ferroparticles in 50%: 50% of ethylene glycol–water mixture base fluids between two disks with the presence of a non-linear thermal radiation heat flux." *Frontiers in Chemistry* 8 (2020): 792. https://doi.org/10.3389/fchem.2020.00792

[18] Hassan Tahir, Umair Khan, Anwarud Din, Yu-Ming Chu, Noor Muhammad, and Xiao-Min Li. "Hybridized two phase ferromagnetic nanofluid with NiZnFe2O4 and MnZnFe2O4." *Ain Shams Engineering Journal* 12, no. 3 (2021): 3063-3070. https://doi.org/10.1016/j.asej.2020.10.026

[19] Kiran Kunwar ChouhanSantosh Chaudhary. "Hybrid ferrofluid flow on a stretching sheet with Stefan blowing and magnetic polarization effects in a porous medium." *Multidiscipline Modeling in Materials and Structures* 20, no. 6 (2024): 1013-1037. https://doi.org/10.1108/MMMS-04-2024-0092

[20] MM Magdy, W Abbas, Kh S Mekheimer, and MS Emam. "Ferro-Fluid Flow and Heat Transfer over Unsteady Stretching Sheet in the Presence of a Nonuniform Magnetic Field." *Journal of Nonlinear Mathematical Physics* 32, no. 1 (2025): 2.

[21] LS Rani TitusAnnamma Abraham. *Flow of Ferrofluid Over an Inclined Stretching Sheet in the Presence of a Magnetic Dipole*. in *Transactions on Engineering Technologies: World Congress on Engineering 2018 26*. 2019. Springer. https://doi.org/10.1007/978-981-32-9531-5_4

[22] Syafiq Zainodin, Anuar Jamaludin, Roslinda Nazar, and Ioan Pop. "Impact of heat source on mixed convection hybrid ferrofluid flow across a shrinking inclined plate subject to convective boundary conditions." *Alexandria Engineering Journal* 87 (2024): 662-681. https://doi.org/10.1016/j.aej.2023.12.057

[23] Hazirah Mohd Azmi, Siti Suzilliana Putri Mohamed Isa, and Norihan Md Arifin. "The boundary layer flow, heat and mass transfer beyond an exponentially stretching/shrinking inclined sheet." *CFD Letters* 12, no. 8 (2020): 98-107. https://doi.org/10.37934/cfdl.12.8.98107

[24] Sumayyah Alabdulhadi, Iskandar Waini, Sameh E Ahmed, and Anuar Ishak. "Hybrid nanofluid flow and heat transfer past an inclined surface." *Mathematics* 9, no. 24 (2021): 3176. https://doi.org/10.3390/math9243176

[25] Raj Kamal TiwariManab Kumar Das. "Heat transfer augmentation in a two-sided lid-driven differentially heated square cavity utilizing nanofluids." *International Journal of heat and Mass transfer* 50, no. 9-10 (2007): 2002-2018. https://doi.org/10.1016/j.ijheatmasstransfer.2006.09.034

[26] Joseph L Neuringer. "Some viscous flows of a saturated ferro-fluid under the combined influence of thermal and magnetic field gradients." *International Journal of Non-Linear Mechanics* 1, no. 2 (1966): 123-137. https://doi.org/10.1016/0020-7462(66)90025-4

[27] Lawrence F Shampine, Jacek Kierzenka, and Mark W Reichelt. "Solving boundary value problems for ordinary differential equations in MATLAB with bvp4c." *Tutorial notes* 2000, no. 1-27 (2000): 4.